THE JOURNAL OF PHYSICAL CHEMISTRY B

Article

pubs.acs.org/JPCB

# Strategy for Enhancement of $^{13}$C-Photo-CIDNP NMR Spectra by Exploiting Fractional $^{13}$C-Labeling of Tryptophan

Wolfgang Eisenreich,[†,¶] Monika Joshi,[†,◆,¶] Boris Illarionov,[‡] Sylwia Kacprzak,[§] Michail Lukaschek,[§] Gerd Kothe,[§] Nediljko Budisa,[∥] Markus Fischer,[‡] Adelbert Bacher,[†] and Stefan Weber*[,§,⊥]

[†]Technische Universität München, Lehrstuhl für Biochemie, Lichtenbergstr. 4, 85748 Garching, Germany

[‡]Universität Hamburg, Institut für Lebensmittelchemie, Bundesstr. 45, 20146 Hamburg, Germany

[§]Albert-Ludwigs-Universität Freiburg, Institut für Physikalische Chemie, Albertstr. 21, 79104 Freiburg, Germany

[∥]Technische Universität Berlin, Institut für Chemie, Müller-Breslau-Str. 10, 10623 Berlin, Germany

[⊥]Freiburg Institute for Advanced Studies (FRIAS), Albertstr. 19, 79104 Freiburg, Germany

Supporting Information

**ABSTRACT:** The photo-CIDNP effect has proven to be useful to strongly enhance NMR signals of photochemically active proteins simply by irradiation with light. The evolving characteristic patterns of enhanced absorptive and emissive NMR lines can be exploited to elucidate the photochemistry and photophysics of light-driven protein reactions. In particular, by the assignment of $^{13}$C NMR resonances, redox-active amino acids may be identified and thereby electron-transfer pathways unraveled, in favorable cases, even with $^{13}$C at natural abundance. If signal enhancement is weak, uniform $^{13}$C isotope labeling is traditionally applied to increase the signal strength of protein $^{13}$C NMR. However, this typically leads to cross relaxation, which transfers light-induced nuclear-spin polarization to adjacent $^{13}$C nuclei, thereby preventing an unambiguous analysis of the photo-CIDNP effect. In this contribution, two isotope labeling strategies are presented; one leads to specific but ubiquitous $^{13}$C labeling in tryptophan, and the other is based on fractional isotope labeling affording sets of isotopologs with low probability of next-neighbor isotope accumulation within individual tryptophan molecules. Consequently, cross relaxation is largely avoided while the signal enhancement by $^{13}$C enrichment is preserved. This results in significantly simplified polarization patterns that are easier to analyze with respect to the generation of light-generated nuclear-spin polarization.

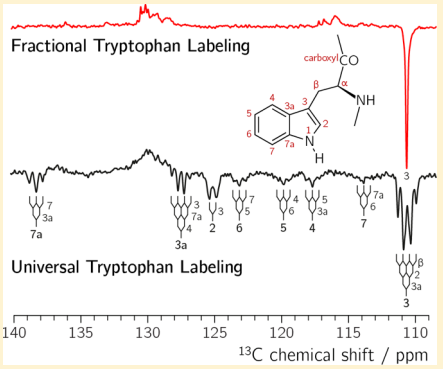


## INTRODUCTION

Chemically induced dynamic nuclear polarization (CIDNP) generated in the course of photochemical electron-transfer reactions between an excited photosensitizer and redox-active amino acid side chains has been frequently used to monitor the exposure of these residues to the protein surroundings and thereby to probe the surface structure and folding of proteins.[1−6] The discovery that photo-CIDNP in photoactive proteins builds up under solid-state conditions opened a new area of applications of this technique to larger protein complexes.[7] Numerous bacterial and plant photosynthetic reaction centers were subjected to $^{15}$N and $^{13}$C magic-angle spinning NMR,[8−11] and photo-CIDNP effects driven by intraprotein electron transfer were detected and analyzed employing three solid-state radical-pair mechanisms (i.e., three-spin mixing,[12−14] differential decay,[15] and differential relaxation).[16,17] By this technique, a high-resolution mapping of the primary donor's electronic structure was achieved.[17−19]

The first nonphotosynthetic protein that was observed to exhibit photo-CIDNP induced by intraprotein electron transfer was a modified LOV2 domain of phototropin,[20] which is a flavin-based photoreceptor that regulates the blue-light-directed growth of *Avena sativa* seedlings.[21−24] In the wild-type protein, the flavin cofactor, upon light excitation, performs covalent adduct formation at C(4a) with a nearby cysteine (C450) residue,[25] via the flavin triplet state;[26] in the C450A mutant, the flavin readily conducts electron transfer with a previously unknown redox partner.[27] Applying $^{13}$C photo-CIDNP under solution-NMR conditions to tryptophan-mutant proteins, a tryptophan residue (W491) was identified by its huge nuclear spin polarization as the electron donor to the flavin.[28,29] Subsequently, photo-CIDNP effects were also reported from the LOV1 domain of phototropin, however, detected under solid-state NMR conditions.[30] Interestingly, a detailed analysis of magnetic-field-dependent NMR enhancement factors revealed that in addition to a radical-pair mechanism, also a new triplet mechanism[31] contributes to photo-CIDNP

**Special Issue:** Wolfgang Lubitz Festschrift

**Received:** July 11, 2015
**Revised:** August 4, 2015
**Published:** August 5, 2015





DOI: 10.1021/acs.jpcb.5b06668
J. Phys. Chem. B 2015, 119, 13934−13943

formation in these proteins, in particular at high magnetic fields.[32]

Flavins are ubiquitously encountered protein cofactors that in many cases undergo light-induced photoreduction reactions with suitable electron donors nearby.[33,34] By exploiting photo-CIDNP effects on flavin cofactors and amino-acid residues, it is in principle possible to unravel electron-transfer pathways even in photoinactive proteins by a procedure similar to the one applied to the LOV2-C450A mutant mentioned above. The latter protein together with the respective LOV1 mutant domain, however, could present rare favorable cases for photo-CIDNP, because the domains are rather small and contain only few tryptophans, W491 and W557 in the case of *Avena sativa* LOV2, the latter being virtually inactive in electron transfer. Larger proteins typically comprise more tryptophan residues and also other redox-active amino acids, which may be individually or simultaneously involved in electron transfer. To identify reactive intermediates in such cases by exploiting light-induced NMR signal polarizations and enhancements, high sensitivity and resolution are required to distinguish different amino-acid residues by means of their specific chemical shifts. Simultaneously, strong photo-CIDNP enhancements are desirable to obtain clear differences between light and dark states, especially when tracking $^{13}C$ resonances at natural abundance. In cases where signal enhancements are weak, uniform $^{13}C$ labeling will be helpful to reduce signal acquisition time; however, due to the resulting multiplet splittings, spectra become more complex because of increased signal overlap, and furthermore, cross relaxation[35] can lead to significant alteration of the light-generated nuclear spin polarization in ubiquitously labeled samples. We present in this contribution a strategy of "fractional" isotope enrichment in protein-bound tryptophans, by means of specific nutrition media, that leads to $^{13}C$ enhancements with simultaneously low probability of nearest next-neighbor $^{13}C$ incorporation. An in-depth study is presented on differently labeled single and double mutants of *Avena sativa* LOV2 that will lay a foundation for a quantitative analysis of the generation of nuclear spin polarization and demonstrate how nonspecific $^{13}C$ labeling may be exploited to simplify photo-CIDNP spectra of more complex systems.

## MATERIALS AND METHODS

**Materials.** [U-$^{13}C_{11}$]Tryptophan was purchased from Cambridge Isotope Laboratories, Andover, MA, U.S.A., and [U-$^{13}C_6$]-, [1-$^{13}C_1$]-, [2-$^{13}C_1$]-, and [3-$^{13}C_1$]glucose were obtained from Isotec, Miamisburg, OH, U.S.A.

The preparation of the recombinant LOV2-C450A mutant domain and double-mutants LOV2-C450A/W491A and LOV2-C450A/W557A (amino acid residues 405 to 559) of *Avena sativa* phototropin follows procedures reported previously.[25] Selected studies have also been performed with a LOV2-C450A domain comprising fewer amino acids (residues 409 to 525) because this sequence contains only one tryptophan.

**Specific [Tryptophan-$^{13}C_{11}$]-LOV2 Domains.** Plasmid constructs specifying double-mutant LOV2 domains were transformed into the tryptophan-deficient *E. coli* hyper-expression strain [*E. coli* ATCC49980 (WP2)].[36,37] The recombinant strains were grown in new minimal medium (NMM)[38] supplemented with [U-$^{13}C_{11}$]tryptophan (10 mg/L).

**Universal and Fractional $^{13}C$ Labeling of LOV2.** Recombinant *E. coli* cells were grown in minimal medium supplied with $^{13}C$-labeled glucose ([1-$^{13}C_1$]-, [2-$^{13}C_1$]-, [3-$^{13}C_1$]- or [U-$^{13}C_{11}$]-labeled). The cultures were incubated at 37 °C with shaking. Isopropyl thiogalactoside was added to a final concentration of 1 mM when the optical density at 600 nm had reached a value of 0.7. Incubation with shaking was continued for 5 h. Cells were harvested by centrifugation and stored at −20 °C.

**Protein Purification.** Recombinant LOV2 domain was purified as described earlier.[20,25]

**Isolation of Tryptophan.** Bacterial cell mass was suspended in 2 M barium hydroxide and was boiled under reflux for 24 h. The solution was neutralized with gaseous carbon dioxide and the precipitate of barium carbonate was removed by centrifugation. The residue was dissolved in 100 mM ammonium formate. The solution was applied to a reversed-phase HPLC column (250 × 16 mm) that was developed with 100 mM ammonium formate. The eluent was monitored photometrically at 278 nm. Fractions were analyzed by thin-layer chromatography (cellulose, butanol/acetic acid/water (30:20:10 v/v), ninhydrin). The retention volume of tryptophan was 192 mL. Fractions were combined, concentrated to dryness under reduced pressure, and dissolved in 5 mL of water. The solution was applied to a reversed-phase HPLC column (250 × 16 mm) that was then developed with 5% aqueous methanol. The retention volume of tryptophan was 88 mL. Fractions were combined and concentrated to dryness under reduced pressure.

**NMR Spectroscopy.** 500-MHz and 600-MHz NMR instrumentation by Bruker was used. $^{13}C$ NMR spectra under blue-light irradiation were acquired as described previously.[20] All $^{13}C$ NMR spectra were recorded at 278 K using a nonselective $\pi/2$ pulse and composite pulse proton decoupling.

**Quantum-Chemical Calculations.** (i) Structure Optimization: Molecular structures of the tryptophan radical and the tryptophan radical cation were modeled by the 3-ethyl-indolyl radical and the 3-ethyl-indolyl radical cation, respectively. Geometry optimization was carried out at the density functional theory (DFT) level using the gradient-corrected BP86 functional[39−41] and a def2-TZVPP Gaussian-type-orbital basis set.[42−44] The Def2-TZVPP auxiliary basis set was used to fit the electron density (RI-DFT approximation).[43] (ii) Hyperfine Tensor Calculations: All hyperfine coupling parameters were computed in the usual nonrelativistic first-order approach, employing the B3LYP hybrid functional[45−47] in combination with the EPR-II basis set[48] that was specifically designed for hyperfine calculations. All calculations were performed with the ORCA program package.[49]

## RESULTS AND DISCUSSION

**Electron Transfer in LOV2 C450A.** The wild-type LOV2 domain of *Avena sativa* phototropin (comprising amino acids 405 to 559) contains two tryptophans, W491 and W557. Residue W491 is 13.7 Å (edge-to-edge distance) apart from the redox-active FMN cofactor, as determined by X-ray crystallography.[50] W557 is located "behind" the helix J$\alpha$ at the C-terminal end of the domain; its distance to FMN, according to an NMR structure, is considerably longer (approximately 35 Å).[51] Upon light irradiation of the C450A mutant protein, the triplet state of FMN ($^3$FMN) is generated,[52] and subsequently, $^3$FMN abstracts an electron from W491 to form the radical-pair state $^3$(FMN$^{\bullet-}$···W491$^{\bullet+}$). Due to conservation of spin-angular momentum in a fast photochemical reaction, this radical pair is generated in its triplet electron-spin configuration.[32] Evidence


DOI: 10.1021/acs.jpcb.5b06668
J. Phys. Chem. B 2015, 119, 13934−13943

for this reactivity came from photo-CIDNP examinations on LOV2-C450A and two double mutants, LOV2-C450A/W491A and LOV2-C450A/W557A: A strongly polarized $^{13}$C NMR signal from C(3) (113.5 ppm, at natural abundance) of a tryptophan residue is observed upon irradiation of LOV2-C450A and LOV2-C450A/W557A but not in LOV2-C450A/W491A.[28] A detailed analysis of the magnetic-field-dependent $^{13}$C NMR enhancement factors of this carbon in the tryptophan residue provided electron spin−spin coupling parameters that are consistent with the above-mentioned distance between $FMN^{\bullet-}$ and $W491^{\bullet+}$.[32] Hence, W491 is the electron donor to $^3$FMN, thus forming the entrance of an electron-transfer channel from the surface of the protein to the cofactor in the core. This observation demonstrates the potential of photo-CIDNP in unraveling electron-transfer pathways among redox-active amino acids in proteins by means of strongly enhanced NMR resonances due to nuclear-spin polarization generated on the individual radical-pair halves. Figure 1 summarizes the primary photochemistry of the LOV2 C450A mutant and the previously identified photo-CIDNP mechanisms that generate nuclear-spin polarization in this domain.[32]

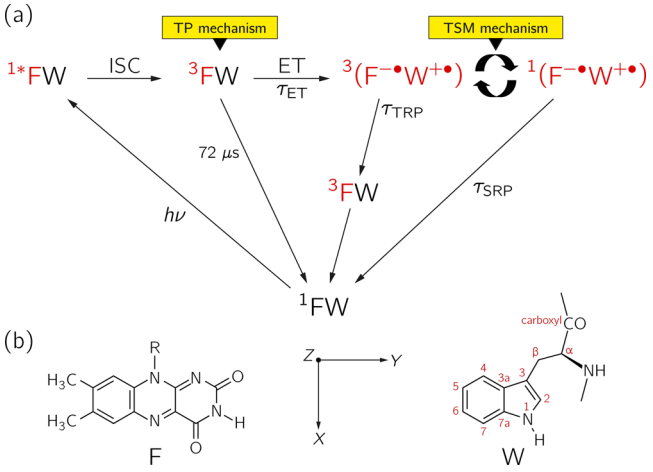


**Figure 1.** (a) Cyclic reaction scheme for the formation of photo-CIDNP in the LOV2-C450A mutant domain of phototropin based on experimental observations by $^{13}$C photo-CIDNP NMR[20,28,32] and time-resolved optical spectroscopy.[26] F: FMN cofactor. W: tryptophan-491 in the apoprotein. ISC: intersystem crossing between excited singlet state of flavin, $^{1*}$F, and triplet state of flavin, $^3$F. TP: triplet polarization mechanism.[31] ET: electron transfer between W491 and $^3$F, assumed to occur with a time constant $\tau_{ET}$ < 5 ns. Under this condition, $^3$($FMN^{\bullet-}$···$W491^{\bullet+}$) acts as an independent photo-CIDNP source.[32] TSM: three-spin mixing mechanism.[12−14] $\tau_{TRP}$: lifetime of $^3$($FMN^{\bullet-}$···$W491^{\bullet+}$). $\tau_{SRP}$: lifetime of $^1$($FMN^{\bullet-}$···$W491^{\bullet+}$). (b) Molecular structures of the redox-active 7,8-dimethyl isoalloxazine ring of flavin and tryptophan. The numbers indicate the positions of the various $^{13}$C hyperfine tensors in $W^{\bullet+}$ (IUPAC numbering scheme).

**$^{13}$C Labeling Strategies.** In the following, labeling strategies are described that were applied to enhance photo-CIDNP $^{13}$C NMR in tryptophan resonances. We refer to the designation "specific labeling" for cases where only tryptophans are enriched while maintaining the residual protein unlabeled (i.e., $^{13}$C at natural abundance), and we use "unspecific labeling" for cases with $^{13}$C enrichment throughout the protein.

**[Tryptophan-$^{13}C_{11}$]-LOV.** To exploit isotope enhancements in photo-CIDNP, we examined double-mutant LOV2-C450A proteins specifically labeled by incorporation of [U-$^{13}C_{11}$]tryptophan. For this purpose, plasmids coding for LOV2-C450A/W491A and LOV2-C450A/W557A were transformed into the tryptophan-dependent *E. coli* strain ATCC49980 (WP2); notably, both plasmids specify LOV domains carrying a single tryptophan. The recombinant strains were grown with a supplement of [U-$^{13}C_{11}$]tryptophan.[36,37] Dark-state solution $^{13}$C NMR spectra of the recombinant proteins are shown in Figure 2. On the basis of $^{13}$C chemical shifts and coupling patterns, all resonances can be assigned to the 11 carbons of tryptophan.

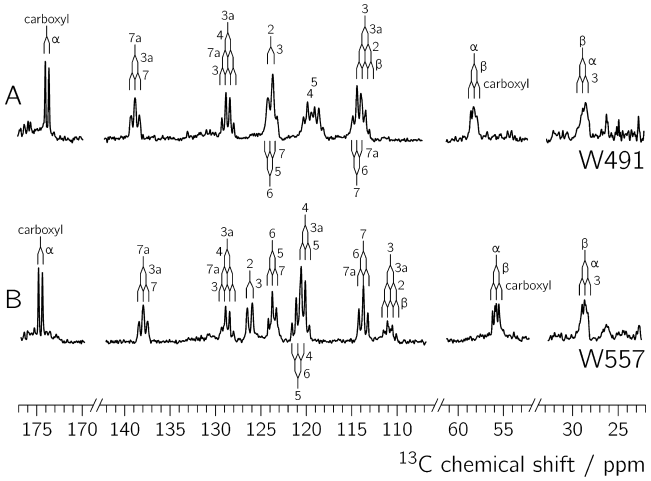


**Figure 2.** Dark-state solution $^{13}$C NMR spectra of C450A/W557A (A) and C450A/W491A (B) double-mutant LOV2 domains. Spectra were recorded at $T$ = 278 K using a nonselective $\pi/2$ pulse and composite pulse proton-decoupling at a magnetic field of 11.8 T. The numbers 2−7a, $\alpha$ and $\beta$ indicate the assignment of the various $^{13}$C signals to carbon atoms in the $^{13}$C-labeled tryptophans (IUPAC numbering scheme).

Both spectra show doublets at low field, which are easily assigned as the carboxylic groups of W491 and W557, respectively, on the basis of chemical shift and multiplicity arguments (coupling constants are 52 and 54 Hz, respectively). The signals of $^{13}$C($\alpha$) and $^{13}$C($\beta$) of the respective tryptophans are also easily identified on the basis of chemical shift and $^{13}$C−$^{13}$C coupling multiplicity. Due to signal overlapping, the multiplets in the aromatic range between 110 and 140 ppm are less easily assigned. In detail, the signals of $^{13}$C(3) and $^{13}$C(7) are both expected at the high-field end of the aromatic signal cluster. In case of the C450A/C491A double mutant, $^{13}$C(3) and $^{13}$C(7) can be easily distinguished on the basis of their respective pseudoquartet and pseudotriplet signatures. The resonances of both carbons appear to overlap in case of the C450A/W557A double mutant. The signal of $^{13}$C(7a) is easily assigned on the basis of its pseudotriplet appearance at the low-field end of the aromatic range. The signals of $^{13}$C(2) and $^{13}$C(3a) can be identified by their respective doublet and pseudoquadruplet signatures. The remaining aromatic carbons $^{13}$C(4), $^{13}$C(5), and $^{13}$C(6) should appear as pseudotriplets. The resonances of $^{13}$C(4) and $^{13}$C(5) strongly overlap in both double mutants due to their broad multiplet structures. In the C450A/W557A double mutant, the signals of $^{13}$C(2) and $^{13}$C(6) are not easily disentangled. Some rather complex patterns of overlapping multiplets are also observed in NMR spectra of blue-light irradiated samples and complicate data analysis (see also below).


DOI: 10.1021/acs.jpcb.5b06668
J. Phys. Chem. B 2015, 119, 13934−13943

When compared to the $^{13}C$ resonances of free tryptophan in buffered aqueous solution (data not shown), [tryptophan-$^{13}C_{11}$]−W491-C450A-LOV exhibits more pronounced deviations from the $^{13}C$-chemical shift values of free tryptophan than [tryptophan-$^{13}C_{11}$]−W557-C450A-LOV, thus implying that the $J\alpha$ helix in between W491 and W557 attenuates solvation in W491 but less so in W557, see Figure 3.

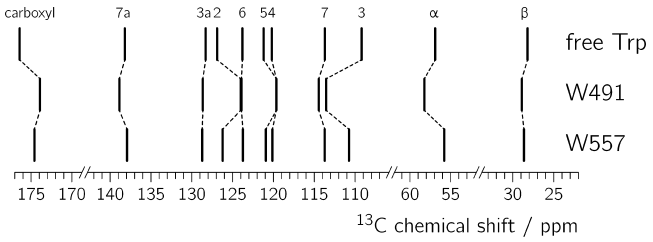


**Figure 3.** $^{13}C$ chemical shifts of free tryptophan in buffered aqueous solution as determined with $^{13}C$ at natural abundance (top), [U-$^{13}C_{11}$]-W491 in the C450A/W557A double-mutant LOV2 domain (middle), and [U-$^{13}C_{11}$]-W557A in the C450A/W491A double mutant LOV2 domain (bottom).

**Universal $^{13}C$ Labeling − U-$^{13}C$]-LOV.** Universally $^{13}C$-labeled LOV2-C450A was prepared using [U-$^{13}C_6$]glucose with the resulting protein carrying [U-$^{13}C_{11}$]tryptophan, and all other amino acids also universally labeled (see Panel D of Figure S1). Due to ubiquitous $^{13}C$−$^{13}C$ multiplet splittings, the resulting $^{13}C$ NMR spectra are very crowded, and individual carbon resonances are hardly resolved. Even in the aromatic region ranging from 100 to slightly above 150 ppm, where most of the tryptophan resonances are expected, significant spectral overlap is observed, even though the LOV2 domain comprises only few aromatic amino acid residues.

**Fractional $^{13}C$ Labeling.** Single-labeled glucoses, on the other hand, afford intricate distributions of $^{13}C$ enrichment in the protein, depending on the type of glucose used, see Panels A to C of Figure S1. To assess the respective $^{13}C$ labeling patterns of tryptophan in these samples, we hydrolyzed *E. coli* biomass grown with single-labeled glucose isotopologs and isolated biosynthetic tryptophan. Each isolated tryptophan sample was then analyzed using $^{13}C$ NMR spectroscopy (see Figure 4). Signal integrals for individual carbons were referenced to the cognate integrals in the spectrum of tryptophan with natural $^{13}C$ abundance under otherwise identical experimental conditions, thus affording $^{13}C$ abundances for each tryptophan carbon position. Notably, the $^{13}C$ signals of the isolated tryptophan samples appear predominantly as singlets (i.e., with few exceptions, $^{13}C$−$^{13}C$ coupling satellites have low intensity). Hence, $^{13}C$ atoms are typically not flanked by $^{13}C$ in next-neighbor positions. This aspect is relevant for the analysis of polarization transfer processes mediated by dipolar cross relaxation (see below).

The protein sample generated in nutrition medium with [1-$^{13}C_1$]glucose afforded a set of tryptophan isotopologs, in which predominantly C(2), C(4), C(7a), and C($\beta$) are $^{13}C$-labeled (see NMR spectrum in Panel C of Figure 4, and Table 1), rather unlikely simultaneously within one molecule but, more likely, in a mixture of tryptophans each being singly enriched with $^{13}C$, e.g., [2-$^{13}C_1$]tryptophan, [4-$^{13}C_1$]-tryptophan, [7a-$^{13}C_1$]tryptophan and [$\beta$-$^{13}C_1$]tryptophan. Doubly enriched tryptophans or tryptophan isotopologs with three or more $^{13}C$ positions within one molecule may also be present in the mixture to a certain (minor) extent, but it is impossible to discern the individual mixture components in terms of labeling degree and positions. Because the tryptophan

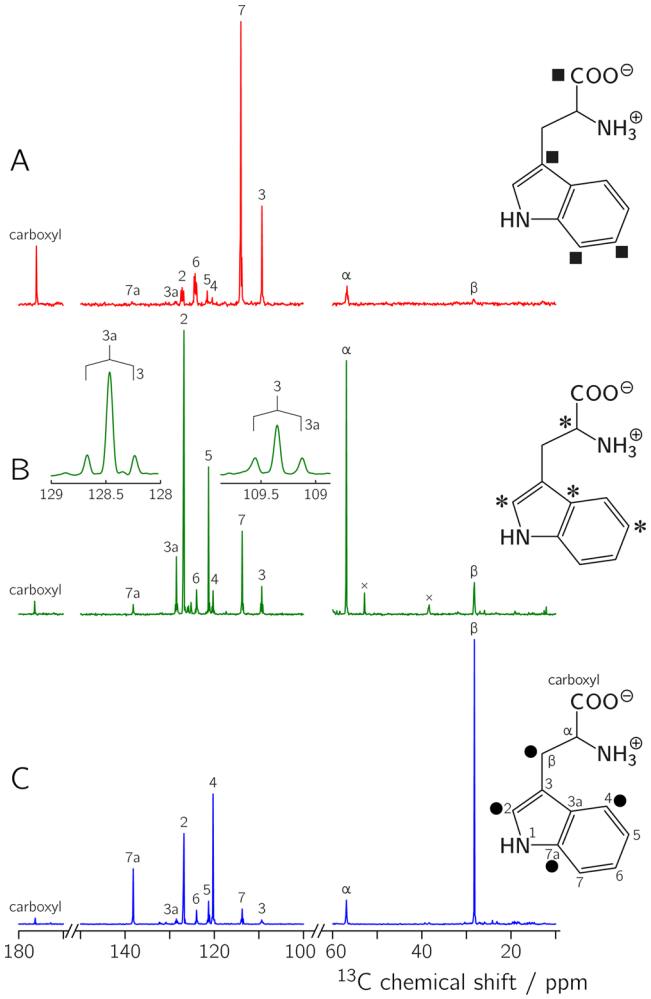


**Figure 4.** $^{13}C$ NMR signals of $^{13}C$ abundance in tryptophan isolated from LOV2 C450A protein grown with [3-$^{13}C_1$]glucose (A), [2-$^{13}C_1$]glucose (B), and [1-$^{13}C_1$]glucose (C). Each spectrum refers to $T$ = 278 K and was recorded using a nonselective $\pi/2$ pulse and composite pulse proton-decoupling at a magnetic field of 11.8 T.

**Table 1. $^{13}C$ Abundance of Tryptophan Isolated from Short LOV2 C450A Domain Grown with [1-$^{13}C_1$]Glucose, [2-$^{13}C_1$]Glucose, and [3-$^{13}C_1$]Glucose[a]**

| | $^{13}C$ abundance/% | | |
|---|---|---|---|
| $^{13}C$ position | [1-$^{13}C_1$]glucose | [2-$^{13}C_1$]glucose | [3-$^{13}C_1$]glucose |
| carboxyl | 3.1 | 7.3 | 32.8 |
| C($\alpha$) | 5.0 | 35.0 | 6.0 |
| C($\beta$) | 33.6 | 8.6 | 1.3 |
| C(2) | 18.1 | 57.5 | 6.5 |
| C(3) | 1.2 | 16.8 | 41.7 |
| C(3a) | 6.2 | 36.5 | 3.0 |
| C(4) | 17.5 | 4.7 | n.d.[b] |
| C(5) | 4.8 | 20.7 | 2.3 |
| C(6) | 2.8 | 5.8 | 13.7 |
| C(7) | 3.3 | 14.2 | 54.5 |
| C(7a) | 29.0 | 6.8 | n.d.[b] |

[a]The individual carbon positions are labeled according to the IUPAC nomenclature. [b]n.d. not determined.



DOI: 10.1021/acs.jpcb.5b06668
J. Phys. Chem. B 2015, 119, 13934−13943

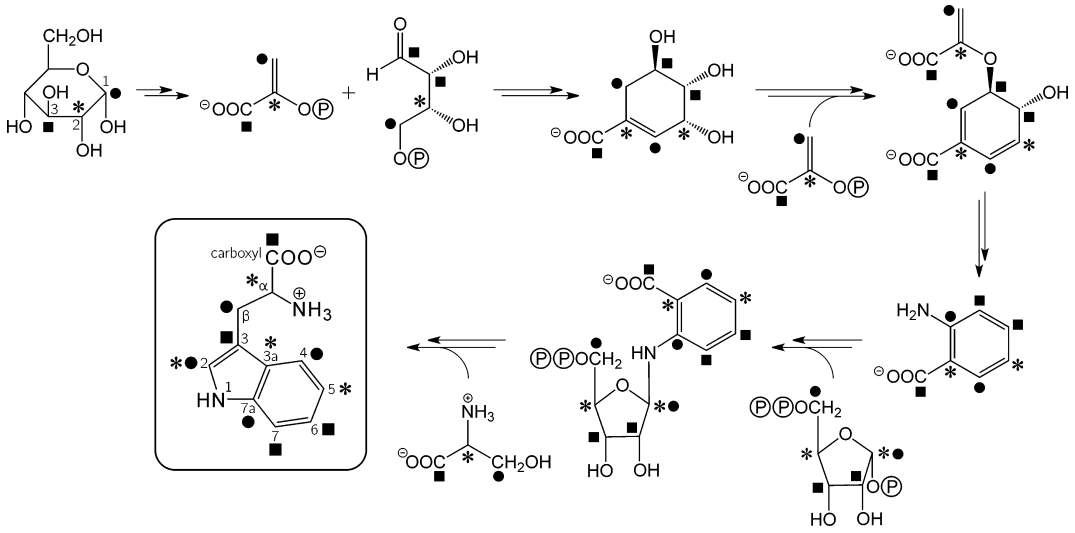

**Figure 5.** Transfer of $^{13}C$ label from [1-$^{13}C_1$]glucose, [2-$^{13}C_1$]glucose, and [3-$^{13}C_1$]glucose into tryptophan via the shikimate pathway.

positions 2, 4, 7a and $\beta$ are all separated from each other by at least one carbon in between them, their $^{13}C$ NMR resonances show up predominantly as singlets with little or no $^{13}C-^{13}C$ coupling satellites. Tryptophan positions that are $^{13}C$ enriched to a much lesser extent but nevertheless to a higher degree than the 1.1% at natural abundance, namely, 3, 3a, 5, 6, 7, carboxyl and $\alpha$, exhibit NMR resonances with more intense multiplet splittings because these sites (except position 6), when $^{13}C$ enriched, quite obviously have a $^{13}C$ as next neighbor. In some cases (e.g., positions 3 and 3a), multiplet splittings to two nonequivalent $^{13}C$ atoms in direct proximity may lead to more complex patterns of low intensity, which are only partly resolved in the NMR data.

The sample generated by growing cells with [2-$^{13}C_1$]glucose afforded a set of tryptophan isotopologs, in which predominantly C(2), C(3a), C(5), and C($\alpha$) are $^{13}C$-labeled (see NMR spectrum in Panel B of Figure 4 and Table 1). The resonances of $^{13}C(2)$, $^{13}C(3a)$, $^{13}C(5)$, and $^{13}C(\alpha)$ have mostly singlet character, because these positions of highest $^{13}C$ enrichment are not directly adjacent. Weak satellites from $^{13}C-^{13}C$ coupling to $^{13}C(3)$ are observed for $^{13}C(3a)$ (see insets in Panel B of Figure 4). These are of course also detected for $^{13}C(3)$, which however has lower $^{13}C$ enrichment as compared to $^{13}C(3a)$.

Finally, medium with [3-$^{13}C_1$]glucose yielded a tryptophan isotopolog mixture with strong $^{13}C$ enrichment in the positions 3, 6, 7, and carboxyl, see Panel A of Figure 4. In this isotopolog set, the probability of finding positions 6 and 7 simultaneously $^{13}C$-enriched is relatively high, and because both positions are directly adjacent, significant multiplet splitting is observed for $^{13}C(6)$ and $^{13}C(7)$. Again, for the position with lower $^{13}C$ enrichment, such as 2 and 3a, multiplets are observed, because once a $^{13}C$ is found at one of these positions, the fraction of molecules carrying $^{13}C$ simultaneously at the adjacent position 3 is rather high.

Table 1 lists the abundance of $^{13}C$ in tryptophan isolated from proteins grown with different singly $^{13}C$-labeled glucoses. Notably, all labeling patterns are well in line with expectations based on central intermediary metabolism and the shikimate pathway in bacteria, see Figure 5.[53,54]

Considering all three sets of tryptophan isotopolog mixtures, it is important to note that significant $^{13}C$ enrichments above the percentage of $^{13}C$ at natural abundance (1.1%) are obtained for all carbon positions in tryptophan, depending on the position of $^{13}C$ enrichment in the carbon source glucose. However, because the overall abundance of $^{13}C$ in tryptophan is typically lower than about 20%, the occurrence of $^{13}C-^{13}C$ couplings between next-neighbor positions, and hence, intensities of multiplet satellites are rather low. These properties shall now be exploited to examine nuclear-spin polarization effects induced by blue-light irradiation of the protein.

**Photo-CIDNP NMR.** Exposure of phototropin's LOV domains to blue light induces reversible photochemistry, by which significant nuclear-spin polarization is generated on those moieties that undergo transient redox changes (i.e., the flavin cofactor that is one-electron reduced and a tryptophan residue within a distance suitable for fast electron transfer that becomes simultaneously one-electron oxidized). The extent of tryptophan $^{13}C$ NMR signal enhancement due to nuclear-spin polarization depends, under the here chosen continuous irradiation conditions, mainly on (i) the type(s) of photo-CIDNP mechanism being active, (ii) the hyperfine properties of magnetic nuclei in tryptophan, (iii) the $^{13}C-^{13}C$ dipolar couplings, by which polarization is transferred from and to neighboring nuclei, and (iv) the relaxation properties of the individual magnetic nuclei, which are responsible for the evolution of polarization.

**Photo-CIDNP NMR – [Tryptophan-$^{13}C_{11}$]-LOV.** Figure 6 depicts photo-CIDNP NMR spectra of the two light-exposed C450A variants that contain only one tryptophan each that is fully $^{13}C$ labeled whereas the other amino acids are unlabeled. Nuclear-spin polarization in LOV2 C450A domains has recently been demonstrated to arise from two solid-state photo-CIDNP mechanisms,[32] specifically the three-spin mixing radical pair mechanism[12−14] and the triplet mechanism;[31] by the latter, however, polarization is generated solely in the flavin cofactor, see also Figure 1. Both mechanisms have in common that they require strongly anisotropic hyperfine interactions for the generation of photo-CIDNP. For a protein in aqueous solution, however, all anisotropic magnetic interactions are modulated by unrestricted rotational protein diffusion. If the protein tumbles such that the correlation time $\tau_C$ satisfies the condition $(\Delta A)^{-1} < \tau_C < (\Delta\sigma)^{-1}$, with $\Delta A$ being the hyperfine



DOI: 10.1021/acs.jpcb.5b06668
J. Phys. Chem. B 2015, 119, 13934−13943

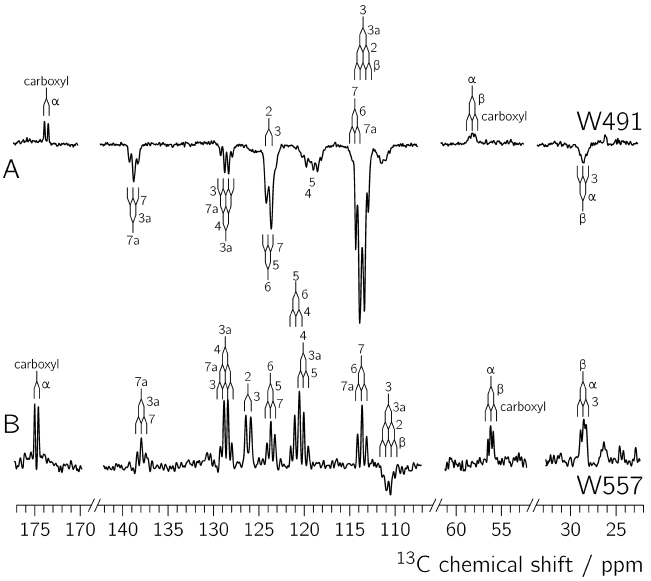


**Figure 6.** Photo-CIDNP $^{13}$C NMR spectra of C450A/W557A (A) and C450A/W491A (B) double-mutant LOV2 domains obtained by continuous blue-light irradiation. Each spectrum refers to $T$ = 278 K and was recorded using a nonselective $\pi/2$ pulse and composite pulse proton-decoupling at a magnetic field of 11.8 T. The numbers 2–7a, $\alpha$ and $\beta$ indicate the assignment of the various $^{13}$C signals to carbon atoms in the $^{13}$C-labeled tryptophans (IUPAC numbering scheme).

anisotropy and $\Delta\sigma$ the chemical-shift anisotropy, chemical-shift anisotropies are averaged to zero, whereas hyperfine anisotropies are largely preserved.[55] Thus, under this condition, one expects to observe liquid-state $^{13}$C NMR spectra with signal enhancements that arise from solid-state photo-CIDNP mechanisms.[32]

The C450A/W557A double mutant comprising [U-$^{13}C_{11}$]-W491 shows all tryptophan $^{13}$C resonances in emission, except for the carboxyl and C($\alpha$) positions, see Panel A of Figure 6. Such a uniform polarization pattern with respect to the sign of NMR enhancement is consistent with the three-spin-mixing radical pair mechanism[12,14] being the dominant mechanism for the generation of nuclear-spin polarization in $^3$(FMN$^{\bullet-}$···W491$^{\bullet+}$).[32] Differential-decay as a further possible radical-pair mechanism can be ruled out by its different sign rule, which predicts that the relative photo-CIDNP enhancement of a given nucleus depends on the sign of the secular hyperfine coupling of the respective $^{13}$C nucleus.[14,15] In the $^3$(FMN$^{\bullet-}$···W491$^{\bullet+}$) radical-pair state, the carboxyl carbon and C($\alpha$) of W491$^{\bullet+}$ carry only minor unpaired electron-spin density, and their resonances are consequently only slightly attenuated in the light as compared to the dark state. C(3) exhibits the most prominent signal enhancement (strong emission) due to the high amount of unpaired electron-spin density in the radical state of W491, and its strong hyperfine anisotropy[56] (i.e., large pseudosecular hyperfine coupling term $B = \Delta A \cdot \sin(\theta_{hf}) \cdot \cos(\theta_{hf})$ with $\Delta A = [A_{ZZ} - (A_{XX} + A_{YY})/2]$, see Table 2).

As compared to the C450A/W557A double mutant, the C450A/W491A protein comprising [U-$^{13}C_{11}$]-W557 exhibits much smaller changes when exposed to blue light, see Panel B of Figure 6. All resonances remain in absorption, except for C(3), which again changes sign (from absorption into emission) in the light state. Apparently, the yield of formation of the radical-pair FMN$^{\bullet-}$···W557$^{\bullet+}$ is quite small, which is not surprising given the larger distance of W557 to FMN. Consequently, the resulting spectrum of the irradiated protein is a superposition of mostly dark-state (hence unpolarized) resonances and a small fraction of emissively polarized resonances of the light state, which leads in the sum to only a small reduction of the dark-state absorptive NMR signals for most nuclei. An exception is C(3) that, for the reasons mentioned above, exhibits an exceptionally strong photo-CIDNP effect, and whose resonance consequently becomes net emissively polarized upon illumination.

Due to the ubiquitous $^{13}$C–$^{13}$C dipolar couplings in protein samples with [U-$^{13}C_{11}$]-W491 or [U-$^{13}C_{11}$]-W557, it is difficult to evaluate the amount of nuclear-spin polarization originally generated by light from that generated by cross relaxation. Hence, reducing $^{13}$C–$^{13}$C dipolar couplings by exploiting fractionally $^{13}$C labeled tryptophans may be beneficial to learn more on the mechanisms of signal enhancement in LOV2. However, because both tryptophans of the LOV2 domain show light-induced signal enhancements, albeit to a quite different extent, we decided to focus in the following on a variant of the protein, in which the N-terminal sequence of the domain is shortened (amino acid residues 409 to 525 of full-length *A. sativa* phototropin) such that only one tryptophan residue, W491, is present. This simplifies assignment and analysis of signal enhancements of the individual NMR resonances of the tryptophan residue.

**Photo-CIDNP NMR – [U-$^{13}$C]-LOV.** Protein isolated from cells grown with uniformly $^{13}$C-labeled glucose affords the entire protein being fully $^{13}$C-labeled, including W491, in contrast to the samples generated from [U-$^{13}C_{11}$]tryptophan, in which only W491 is $^{13}$C labeled. Hence, photo-CIDNP spectra of such a sample are less "pure" as compared to spectra of the

**Table 2. DFT-Calculated $^{13}$C Hyperfine Couplings of Neutral and Cationic Tryptophanyl Radicals in MHz[a]**

| | W$^{\bullet+}$ | | | | | W$^{\bullet}$ | | | | |
|---|---|---|---|---|---|---|---|---|---|---|
| | $A_{XX}$ | $A_{YY}$ | $A_{ZZ}$ | $A_{iso}$ | $\Delta A$ | $A_{XX}$ | $A_{YY}$ | $A_{ZZ}$ | $A_{iso}$ | $\Delta A$ |
| $^{13}$C(2) | −14.6 | −16.4 | +36.2 | +1.7 | +51.7 | −22.3 | −24.3 | −36.0 | −27.5 | −12.7 |
| $^{13}$C(3) | −2.1 | −4.0 | +77.8 | +23.9 | +80.9 | +6.1 | +6.6 | +132.9 | +48.5 | +126.6 |
| $^{13}$C(3a) | −15.1 | −19.0 | −31.8 | −22.0 | −14.8 | −19.8 | −23.6 | −38.8 | −27.4 | −17.1 |
| $^{13}$C(4) | +2.1 | +2.5 | +53.8 | +19.5 | +51.5 | +2.4 | +2.6 | +42.5 | +15.8 | +40.0 |
| $^{13}$C(5) | −9.9 | −11.1 | −23.8 | −14.9 | −13.3 | −9.1 | −10.1 | −17.6 | −12.3 | −8.0 |
| $^{13}$C(6) | −0.1 | −1.0 | +36.5 | +11.8 | +37.1 | −0.2 | +0.6 | +33.3 | +11.2 | +33.1 |
| $^{13}$C(7) | −5.8 | −6.9 | +9.0 | −1.2 | +15.4 | −3.8 | −6.2 | −7.6 | −5.9 | −2.6 |
| $^{13}$C(7a) | −2.1 | +3.0 | −4.5 | −1.2 | −5.0 | −3.8 | −5.9 | +9.4 | −0.1 | +14.3 |

[a]Hyperfine anisotropies were calculated according to the equation $\Delta A = A_{ZZ} - (A_{XX} + A_{YY})/2$. The individual carbon positions are labeled according to the IUPAC nomenclature for tryptophan. For computational details, see the Methods section.



DOI: 10.1021/acs.jpcb.5b06668
J. Phys. Chem. B 2015, 119, 13934–13943

specifically $^{13}$C-labeled tryptophan variants because (unpolarized) resonances from other (aromatic) amino acids contribute to the spectrum in the aromatic region to some extent, see Panel D of Figure 7. Nevertheless, the sample generated from

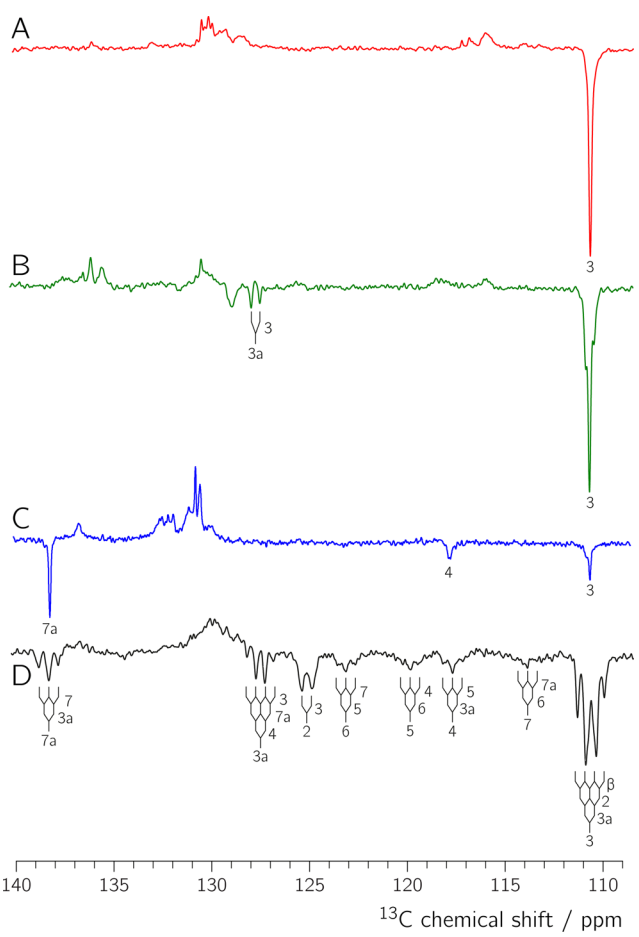


**Figure 7.** Photo-CIDNP $^{13}$C NMR spectra of LOV2 C450A mutant proteins grown with [3-$^{13}C_1$]glucose[29] (A), [2-$^{13}C_1$]glucose (B), [1-$^{13}C_1$]glucose (C), and [U-$^{13}C_6$]glucose (D).[29] Each spectrum refers to $T$ = 278 K and was recorded using a nonselective $\pi/2$ pulse and composite pulse proton-decoupling while continuously irradiating with blue-light at a magnetic field of 11.8 T.

uniformly $^{13}$C-labeled glucose shows the same overall trend on continuous irradiation with blue light: emissive polarization of the resonances of all aromatic carbons of W491, in particular $^{13}$C(3), is observed; however, severe spectral overlap due to rich multiplet splitting is ubiquitous. This reduces the overall amplitude of polarized transitions as compared to the background of noise and signals from amino acids that do not show any photo-CIDNP effect.

**Photo-CIDNP NMR – Fractionally $^{13}$C-Labeled LOV.** In contrast to the universally labeled LOV, the light spectra of samples generated from singly $^{13}$C-labeled glucoses exhibit drastically reduced $^{13}$C–$^{13}$C multiplet splittings, and hence more "isolated" and intense (singlet-type) photo-CIDNP signals are detected, see Panels A to C of Figure 7. Only C(4) and the quaternary indole carbons C(3), C(3a), and C(7a) give rise to detectable emissive signals in protein samples, where the indole rings carry single $^{13}$C labels but no universal labeling. Low levels of labeling cannot explain this finding, because each of the aromatic carbons shows at least 14% $^{13}$C enrichment in at least one of the labeled specimens. Thus, C(2) and C(5) are enriched to about 57 and 21% in the sample from [1-$^{13}C_1$]glucose, and C(7) and C(6) are enriched to about 54 and 14%, respectively, in the sample from [3-$^{13}C_1$]glucose, see Table 1, but none of these carbons shows up in the respective light-state spectra. This is clear evidence that the nuclear-spin polarization on C(2), C(5), C(6), and C(7), observed in continuously irradiated samples with ubiquitously $^{13}$C labeled tryptophans, is generated by cross relaxation from those carbons that acquired very strong polarization, in particular C(3). Any polarization that is directly generated on C(2), C(5), C(6), and C(7) is either small, due to their for photo-CIDNP signal enhancement unfavorable hyperfine properties, and/or escapes detection under continuous illumination conditions because of fast polarization decay.

The carbons C(3), C(3a), C(4), and C(7a) show emissive polarization to varying extents, depending on their abundance in the three sets of tryptophan isotopologs. C(3) exhibits by far the strongest hyperfine anisotropy $\Delta A$ both in the neutral (W491$^{\bullet}$) and the cationic tryptophan (W491$^{\bullet+}$) radical (see Table 2). Among all carbons in the benzene ring of the indole moiety, C(4) accumulates the highest unpaired electron-spin density in the radical state of tryptophan, regardless of whether it is neutral or cationic, and consequently has a relatively large isotropic hyperfine coupling component[57] concomitant with strong hyperfine anisotropy (see Table 2),[56] which significantly enhances its photo-CIDNP effect.

C(3a) also exhibits emissive nuclear-spin polarization; however, only the "satellite lines" flanking the resonance position of the uncoupled C(3a) NMR transition, which arise from $^{13}$C–$^{13}$C coupling with $^{13}$C(3), are observed. Therefore, we conclude that C(3a) receives its polarization solely by cross relaxation, namely, in tryptophan modules in which C(3a) and the neighboring C(3) are both $^{13}$C labeled. Nuclear-spin polarization that is generated on $^{13}$C(3a) by "direct" coupling to the light-induced unpaired electron spin on W491, which is delocalized over the indole ring, is not observed under the chosen illumination conditions. This is most likely due to the only moderate hyperfine anisotropy of $^{13}$C(3a), see Table 2.

Photo-CIDNP on C(7a) is observed only in the sample generated from [1-$^{13}C_1$]glucose, in which strong accumulation of $^{13}$C at position 7a is found. According to our quantum-chemical calculations, $^{13}$C(7a) has a very weak isotropic hyperfine coupling and only minor hyperfine anisotropy in W491$^{\bullet+}$; the neutral W491$^{\bullet}$ radical, however, exhibits considerably stronger hyperfine anisotropy at position 7a, comparable to that of $^{13}$C(3a). This notion of a neutral instead of a cationic W491 radical in the course of photoinduced charge transfer in LOV2 C450A clearly needs further substantiation by alternative methods. At present it is unclear why C(7a) exhibits a singlet-type emissive NMR resonance (indicative of nuclear-spin polarization devoid of $^{13}$C–$^{13}$C cross relaxation) whereas C(3a) does not, and instead, shows its polarization governed exclusively by transfer from $^{13}$C(3). Studies along these lines need to be carried out preferentially using specifically labeled tryptophans with nonuniform $^{13}$C labeling and perhaps also $^{14}$N-to-$^{15}$N substitution.

In all partially $^{13}$C-labeled samples, C(3) exhibits by far the strongest photo-CIDNP effect. Even in the protein produced from [1-$^{13}C_1$]glucose, in which its enrichment is only slightly above the level of natural abundance, clear emissive polarization is observed, see Panel C of Figure 7, consistent with previous observations of this resonance in unlabeled proteins.[20,28,32]


DOI: 10.1021/acs.jpcb.5b06668
J. Phys. Chem. B 2015, 119, 13934–13943

Hence, due to its favorable photo-CIDNP properties, exceptionally strong $^{13}C$ isotropic hyperfine coupling with pronounced hyperfine anisotropy, $^{13}C(3)$ has the potential to act as a marker nucleus for the identification of photo-CIDNP in other proteins. The intensity of this marker signal can be further significantly enhanced upon fractional $^{13}C$ labeling from cell growth with [2-$^{13}C_1$]glucose or [3-$^{13}C_1$]glucose, by which $^{13}C$ abundances of 16.8 and 41.7% are reached, respectively, see Panels B and A of Figure 7. In both samples, the singlet character of the C(3) resonance is largely preserved. Only in protein prepared from [2-$^{13}C_1$]glucose, the C(3) resonance is slightly broadened by $^{13}C-^{13}C$ coupling with $^{13}C(3a)$ because the enrichment of the latter (36.5%) in this sample is quite strong and the probability of finding $^{13}C(3)$ and $^{13}C(3a)$ simultaneously in W491 is consequently rather high (see above), see Panel B of Figure 7.

It is beyond the scope of this contribution to quantitatively analyze the observed photo-CIDNP intensities, because experimental hyperfine data on $^{13}C$ in neutral and cationic tryptophan radicals are scarce; whereas isotropic $^{13}C$ hyperfine values deduced from time-resolved CIDNP studies on isolated tryptophan radicals have been presented some time ago,[57] and $^{13}C$ hyperfine anisotropies are, to the best of our knowledge, undetermined so far.

**Evaluation of Tryptophan Labeling Strategies for Photo-CIDNP.** The present applications of two tryptophan labeling strategies, (i) introduction of tryptophan isotopologs into a protein via a tryptophan-deficient *E. coli* strain (selective labeling), and (ii) (fractional) tryptophan $^{13}C$ labeling by growing cells with singly $^{13}C$-labeled glucoses, beautifully demonstrate their strengths and weaknesses in photo-CIDNP $^{13}C$ NMR studies. Clearly, the possibility of incorporating virtually any specific tryptophan isotopolog into a protein potentially offers the highest flexibility for exploiting isotope effects by NMR, both in the dark and light state, in particular for proteins with only few tryptophans in their amino-acid sequence. Presently, however, only ubiquitously $^{13}C$-labeled tryptophan and [2-$^{13}C_1$]tryptophan are commercially available. Of all potential isotopologs, [U-$^{13}C_{11}$]tryptophan leads to the strongest "spreading out" of light-induced nuclear-spin polarization due to cross relaxation thereby complicating quantitative analysis. Hence, this labeling strategy exhibits its strengths predominantly in dark-state NMR to identify chemical shifts of the individual resonances and the multiplet splittings between the various $^{13}Cs$ in the residue that allow for an unambiguous signal assignment. As more specifically labeled tryptophan isotopologs become available, this method may increasingly gain in value also in studies of photo-CIDNP effects.

Fractional labeling of tryptophan by growing protein with selectively $^{13}C$-labeled glucoses, on the other hand, provides a means to increase the $^{13}C$ enrichment of all carbons in tryptophan significantly beyond the value of natural abundance, depending on the type of glucose used to an average level of about 10−20%. This dramatically enhances the detection sensitivity for the individual carbons while still preserving the singlet-type nature of resonances both in dark-state as well as in photo-CIDNP NMR. Although not all carbons of tryptophan appear spin polarized in experiments with continuous blue-light irradiation, C(3) and C(7a) experience exceptionally strong signal enhancements in samples generated from [3-$^{13}C_1$]-glucose and [1-$^{13}C_1$]glucose, respectively. Hence, these resonances may serve as marker signals in proteins in which photo-CIDNP effects shall be traced. Additionally, partial $^{13}C$ labeling of tryptophan to a moderately high level will simplify quantitative analysis of the generation of light-induced nuclear spin polarization due to strongly attenuating cross relaxation pathways.

## CONCLUSIONS

We present two strategies of introducing $^{13}C$ into tryptophan, thereby enhancing detection sensitivity for photo-CIDNP NMR on selected marker lines by more than 1 order of magnitude. In particular, $^{13}C$-labeling of samples by feeding selectively labeled glucoses for protein production provides the means of increasing the $^{13}C$ abundance while maintaining probabilities for cross relaxation in tryptophan at a low level. A quantitative analysis of photo-CIDNP in LOV2 domains appears now feasible using the synthetic approaches presented here. The labeling strategies might furthermore be helpful in future photo-CIDNP examinations of larger proteins to unravel electron-transfer pathways and to achieve a quantitative analysis of nuclear-spin polarization effects.

## ASSOCIATED CONTENT

### Supporting Information

The Supporting Information is available free of charge on the ACS Publications website at DOI: 10.1021/acs.jpcb.5b06668.

Dark-state solution $^{13}C$ NMR spectra of LOV2 C450A samples generated from nutrition medium with [U-$^{13}C_6$]-, [1-$^{13}C_1$]-, [2-$^{13}C_1$]-, and [3-$^{13}C_1$]glucose (PDF)

## AUTHOR INFORMATION


### Corresponding Author

*E-mail: stefan.weber@physchem.uni-freiburg.de.

### Present Address

♦Department of Biomedical and Molecular Sciences, Queen's University, Kingston, Ontario, Canada.

### Author Contributions

¶W.E. and M.J. contributed equally.


### Notes

The authors declare no competing financial interest.

## ACKNOWLEDGMENTS

We thank Jens Haller and Jakob Wörner for their assistance in analyzing the NMR data. This work was supported by grants of the Deutsche Forschungsgemeinschaft (DFG), WE 2376/4-1 and FI 824/6-1, and the Hans-Fischer-Gesellschaft e.V. (München). NMR instrumentation at the Institute of Physical Chemistry of the Albert-Ludwigs-University of Freiburg was cofinanced by the DFG (INST 39/933-1 FUGG) and the Baden-Württemberg Stiftung (Struktur- und Innovationsfonds für die Forschung, SI-BW).

## REFERENCES

(1) Kaptein, R.; Dijkstra, K.; Nicolay, K. Laser Photo-CIDNP as a Surface Probe for Proteins in Solution. *Nature (London, U. K.)* **1978**, *274*, 293−294.

(2) Hore, P. J.; Broadhurst, R. W. Photo-CIDNP of Biopolymers. *Prog. Nucl. Magn. Reson. Spectrosc.* **1993**, *25*, 345−402.

(3) Mok, K. H.; Hore, P. J. Photo-CIDNP NMR Methods for Studying Protein Folding. *Methods* **2004**, *34*, 75−87.



DOI: 10.1021/acs.jpcb.5b06668
*J. Phys. Chem. B* 2015, 119, 13934−13943

(4) Goez, M. Photo-CIDNP Spectroscopy. In *Annual Reports on NMR Spectroscopy*; Webb, G. A., Ed.; Elsevier: Amsterdam, 2009; Vol. *66*, pp 77−147.
(5) Maeda, K.; Lyon, C. E.; Lopez, J. J.; Cemazar, M.; Dobson, C. M.; Hore, P. J. Improved Photo-CIDNP Methods for Studying Protein Structure and Folding. *J. Biomol. NMR* **2000**, *16*, 235−244.
(6) Wirmer, J.; Kühn, T.; Schwalbe, H. Millisecond Time Resolved Photo-CIDNP NMR Reveals a Non-Native Folding Intermediate on the Ion-Induced Refolding Pathway of Bovine $\alpha$-Lactalbumin. *Angew. Chem., Int. Ed.* **2001**, *40*, 4248−4251.
(7) Zysmilich, M. G.; McDermott, A. Photochemically Induced Dynamic Nuclear Polarization in the Solid-State $^{15}$N Spectra of Reaction Centers from Photosynthetic Bacteria *Rhodobacter sphaeroides* R-26. *J. Am. Chem. Soc.* **1994**, *116*, 8362−8363.
(8) Zysmilich, M. G.; McDermott, A. Natural Abundance Solid-State Carbon NMR Studies of Photosynthetic Reaction Centers with Photoinduced Polarization. *Proc. Natl. Acad. Sci. U. S. A.* **1996**, *93*, 6857−6860.
(9) Alia; Roy, E.; Gast, P.; van Gorkom, H. J.; de Groot, H. J. M.; Jeschke, G.; Matysik, J. Photochemically Induced Dynamic Nuclear Polarization in Photosystem I of Plants Observed by $^{13}$C Magic-Angle Spinning NMR. *J. Am. Chem. Soc.* **2004**, *126*, 12819−12826.
(10) Prakash, S.; Alia; Gast, P.; de Groot, H. J. M.; Matysik, J.; Jeschke, G. Photo-CIDNP MAS NMR in Intact Cells of *Rhodobacter sphaeroides* R26: Molecular and Atomic Resolution at Nanomolar Concentration. *J. Am. Chem. Soc.* **2006**, *128*, 12794−12799.
(11) Roy, E.; Rohmer, T.; Gast, P.; Jeschke, G.; Alia, A.; Matysik, J. Characterization of the Primary Radical Pair in Reaction Centers of *Heliobacillus mobilis* by $^{13}$C Photo-CIDNP MAS NMR. *Biochemistry* **2008**, *47*, 4629−4635.
(12) Jeschke, G. A New Mechanism for Chemically Induced Dynamic Nuclear Polarization in the Solid State. *J. Am. Chem. Soc.* **1998**, *120*, 4425−4429.
(13) Kothe, G.; Bechtold, M.; Link, G.; Ohmes, E.; Weidner, J.-U. Pulsed EPR Detection of Light-Generated Nuclear Coherences in Photosynthetic Reaction Centers. *Chem. Phys. Lett.* **1998**, *283*, 51−60.
(14) Jeschke, G.; Matysik, J. A Reassessment of the Origin of Photochemically Induced Dynamic Nuclear Polarization Effects in Solids. *Chem. Phys.* **2003**, *294*, 239−255.
(15) Polenova, T.; McDermott, A. E. A Coherent Mixing Mechanism Explains the Photoinduced Nuclear Polarization in Photosynthetic Reaction Centers. *J. Phys. Chem. B* **1999**, *103*, 535−548.
(16) McDermott, A.; Zysmilich, M. G.; Polenova, T. Solid State NMR Studies of Photoinduced Polarization in Photosynthetic Reaction Centers: Mechanism and Simulations. *Solid State Nucl. Magn. Reson.* **1998**, *11*, 21−47.
(17) Thamarath, S. S.; Bode, B. E.; Prakash, S.; Gupta, K. B. S. S.; Alia, A.; Jeschke, G.; Matysik, J. Electron Spin Density Distribution in the Special Pair Triplet of *Rhodobacter sphaeroides* R26 Revealed by Magnetic Field Dependence of the Solid-State Photo-CIDNP Effect. *J. Am. Chem. Soc.* **2012**, *134*, 5921−5930.
(18) Schulten, E. A. M.; Matysik, J.; Alia; Kiihne, S.; Raap, J.; Lugtenburg, J.; Gast, P.; Hoff, A. J.; de Groot, H. J. M. $^{13}$C MAS NMR and Photo-CIDNP Reveal a Pronounced Asymmetry in the Electronic Ground State of the Special Pair of *Rhodobacter sphaeroides* Reaction Centers. *Biochemistry* **2002**, *41*, 8708−8717.
(19) Daviso, E.; Prakash, S.; Alia, A.; Gast, P.; Neugebauer, J.; Jeschke, G.; Matysik, J. The Electronic Structure of the Primary Electron Donor of Reaction Centers of Purple Bacteria at Atomic Resolution as Observed by Photo-CIDNP $^{13}$C NMR. *Proc. Natl. Acad. Sci. U. S. A.* **2009**, *106*, 22281−22286.
(20) Richter, G.; Weber, S.; Römisch, W.; Bacher, A.; Fischer, M.; Eisenreich, W. Photochemically Induced Dynamic Nuclear Polarization in a C450A Mutant of the LOV2 Domain of the *Avena sativa* Blue-Light Receptor Phototropin. *J. Am. Chem. Soc.* **2005**, *127*, 17245−17252.
(21) Demarsy, E.; Fankhauser, C. Higher Plants Use LOV to Perceive Blue Light. *Curr. Opin. Plant Biol.* **2009**, *12*, 69−74.
(22) Christie, J. M.; Gawthorne, J.; Young, G.; Fraser, N. J.; Roe, A. J. LOV to BLUF: Flavoprotein Contributions to the Optogenetic Toolkit. *Mol. Plant* **2012**, *5*, 533−544.
(23) Hohm, T.; Preuten, T.; Fankhauser, C. Phototropism: Translating Light into Directional Growth. *Am. J. Bot.* **2013**, *100*, 47−59.
(24) Liscum, E.; Askinosie, S. K.; Leuchtman, D. L.; Morrow, J.; Willenburg, K. T.; Coats, D. R. Phototropism: Growing towards an Understanding of Plant Movement. *Plant Cell* **2014**, *26*, 38−55.
(25) Salomon, M.; Eisenreich, W.; Dürr, H.; Schleicher, E.; Knieb, E.; Massey, V.; Rüdiger, W.; Müller, F.; Bacher, A.; Richter, G. An Optomechanical Transducer in the Blue Light Receptor Phototropin from *Avena sativa*. *Proc. Natl. Acad. Sci. U. S. A.* **2001**, *98*, 12357−12361.
(26) Swartz, T. E.; Corchnoy, S. B.; Christie, J. M.; Lewis, J. W.; Szundi, I.; Briggs, W. R.; Bogomolni, R. A. The Photocycle of a Flavin-Binding Domain of the Blue Light Photoreceptor Phototropin. *J. Biol. Chem.* **2001**, *276*, 36493−36500.
(27) Kay, C. W. M.; Kuppig, A.; Schleicher, E.; Bacher, A.; Richter, G.; Weber, S. Photochemistry of a C450A Mutant of the LOV2 Domain in Phototropin: Detection of a Light-Induced Neutral Flavin Radical by EPR Spectroscopy. In *Flavins and Flavoproteins 2002*; Chapman, S., Perham, R., Scrutton, N., Eds.; Rudolf Weber Agency for Scientific Publications: Berlin, 2002; pp 707−712.
(28) Eisenreich, W.; Joshi, M.; Weber, S.; Bacher, A.; Fischer, M. Natural Abundance Solution $^{13}$C NMR Studies of a Phototropin with Photoinduced Polarization. *J. Am. Chem. Soc.* **2008**, *130*, 13544−13545.
(29) Eisenreich, W.; Fischer, M.; Römisch-Margl, W.; Joshi, M.; Richter, G.; Bacher, A.; Weber, S. Tryptophan $^{13}$C Nuclear-Spin Polarization Generated by Intraprotein Electron Transfer in a LOV2 Domain of the Blue-Light Receptor Phototropin. *Biochem. Soc. Trans.* **2009**, *37*, 382−386.
(30) Thamarath, S. S.; Heberle, J.; Hore, P. J.; Kottke, T.; Matysik, J. Solid-State Photo-CIDNP Effect Observed in Phototropin LOV1-C57S by $^{13}$C Magic-Angle Spinning NMR Spectroscopy. *J. Am. Chem. Soc.* **2010**, *132*, 15542−15543.
(31) Kothe, G.; Yago, T.; Weidner, J.-U.; Link, G.; Lukaschek, M.; Lin, T.-S. Quantum Oscillations and Polarization of Nuclear Spins in Photoexcited Triplet States. *J. Phys. Chem. B* **2010**, *114*, 14755−14762.
(32) Kothe, G.; Lukaschek, M.; Link, G.; Kacprzak, S.; Illarionov, B.; Fischer, M.; Eisenreich, W.; Bacher, A.; Weber, S. Detecting a New Source for Photochemically Induced Dynamic Nuclear Polarization in the LOV2 Domain of Phototropin by Magnetic-Field Dependent $^{13}$C NMR Spectroscopy. *J. Phys. Chem. B* **2014**, *118*, 11622−11632.
(33) Massey, V.; Stankovich, M.; Hemmerich, P. Light-Mediated Reduction of Flavoproteins with Flavins as Catalysts. *Biochemistry* **1978**, *17*, 1−8.
(34) Heelis, P. F.; Phillips, G. O. Photoreduction Reactions of Flavin Coenzymes − a Laser Flash Photolysis Study. *Photobiochem. Photobiophys.* **1979**, *1*, 63−70.
(35) Hore, P. J.; Egmond, M. R.; Edzes, H. T.; Kaptein, R. Cross-Relaxation Effects in the Photo-CIDNP Spectra of Amino Acids and Proteins. *J. Magn. Reson.* **1982**, *49*, 122−150.
(36) Minks, C.; Huber, R.; Moroder, L.; Budisa, N. Atomic Mutations at the Single Tryptophan Residue of Human Recombinant Annexin V: Effects on Structure, Stability, and Activity. *Biochemistry* **1999**, *38*, 10649−10659.
(37) Budisa, N.; Alefelder, S.; Bae, J. H.; Golbik, R.; Minks, C.; Huber, R.; Moroder, L. Proteins with $\beta$-(Thienopyrrolyl)Alanines as Alternative Chromophores and Pharmaceutically Active Amino Acids. *Protein Sci.* **2001**, *10*, 1281−1292.
(38) Budisa, N.; Karnbrock, W.; Steinbacher, S.; Humm, A.; Prade, L.; Neuefeind, T.; Moroder, L.; Huber, R. Bioincorporation of Telluromethionine into Proteins: A Promising New Approach for X-Ray Structure Analysis of Proteins. *J. Mol. Biol.* **1997**, *270*, 616−623.
(39) Becke, A. D. Density-Functional Exchange-Energy Approximation with Correct Asymptotic Behavior. *Phys. Rev. A: At., Mol., Opt. Phys.* **1988**, *38*, 3098−3100.


DOI: 10.1021/acs.jpcb.5b06668
*J. Phys. Chem. B* 2015, 119, 13934−13943

(40) Perdew, J. P. Density-Functional Approximation for the Correlation Energy of the Inhomogeneous Electron Gas. *Phys. Rev. B: Condens. Matter Mater. Phys.* **1986**, *33*, 8822−8824.
(41) Perdew, J. P. Erratum: Density-Functional Approximation for the Correlation Energy of the Inhomogeneous Electron Gas [Phys. Rev. B 33, 8822 (1986)]. *Phys. Rev. B: Condens. Matter Mater. Phys.* **1986**, *34*, 7406.
(42) Schäfer, A.; Horn, H.; Ahlrichs, R. Fully Optimized Contracted Gaussian Basis Sets for Atoms Li to Kr. *J. Chem. Phys.* **1992**, *97*, 2571−2577.
(43) Weigend, F.; Ahlrichs, R. Balanced Basis Sets of Split Valence, Triple Zeta Valence and Quadruple Zeta Valence Quality for H to Rn: Design and Assessment of Accuracy. *Phys. Chem. Chem. Phys.* **2005**, *7*, 3297−3305.
(44) Weigend, F.; Häser, M.; Patzelt, H.; Ahlrichs, R. RI-MP2: Optimized Auxiliary Basis Sets and Demonstration of Efficiency. *Chem. Phys. Lett.* **1998**, *294*, 143−152.
(45) Lee, C.; Yang, W.; Parr, R. G. Development of the Colle-Salvetti Correlation-Energy Formula into a Functional of the Electron Density. *Phys. Rev. B: Condens. Matter Mater. Phys.* **1988**, *37*, 785−789.
(46) Becke, A. D. Density-Functional Thermochemistry. III. The Role of Exact Exchange. *J. Chem. Phys.* **1993**, *98*, 5648−5652.
(47) Miehlich, B.; Savin, A.; Stoll, H.; Preuss, H. Results Obtained with the Correlation Energy Density Functionals of Becke and Lee, Yang and Parr. *Chem. Phys. Lett.* **1989**, *157*, 200−206.
(48) Barone, V. Structure, Magnetic Properties and Reactivities of Open-Shell Species from Density Functional and Self-Consistent Hybrid Methods. In *Recent Advances in Density-Functional Methods*; Chong, D. P., Ed.; World Scientific Publishing: Singapore, 1996; Vol. *1*, pp 287−334.
(49) Neese, F. The ORCA Program System. *WIREs Comput. Mol. Sci.* **2012**, *2*, 73−78.
(50) Halavaty, A. S.; Moffat, K. N- and C-Terminal Flanking Regions Modulate Light-Induced Signal Transduction in the LOV2 Domain of the Blue Light Sensor Phototropin 1 from *Avena sativa*. *Biochemistry* **2007**, *46*, 14001−14009.
(51) Harper, S. M.; Neil, L. C.; Gardner, K. H. Structural Basis of a Phototropin Light Switch. *Science* **2003**, *301*, 1541−1544.
(52) Schleicher, E.; Kowalczyk, R. M.; Kay, C. W. M.; Hegemann, P.; Bacher, A.; Fischer, M.; Bittl, R.; Richter, G.; Weber, S. On the Reaction Mechanism of Adduct Formation in LOV Domains of the Plant Blue-Light Receptor Phototropin. *J. Am. Chem. Soc.* **2004**, *126*, 11067−11076.
(53) Herrmann, K. M. The Shikimate Pathway: Early Steps in the Biosynthesis of Aromatic Compounds. *Plant Cell* **1995**, *7*, 907−919.
(54) Herrmann, K. M.; Weaver, L. M. The Shikimate Pathway. *Annu. Rev. Plant Physiol. Plant Mol. Biol.* **1999**, *50*, 473−503.
(55) Daviso, E.; Janssen, G. J.; Alia, A.; Jeschke, G.; Matysik, J.; Tessari, M. A 10000-Fold Nuclear Hyperpolarization of a Membrane Protein in the Liquid Phase via a Solid-State Mechanism. *J. Am. Chem. Soc.* **2011**, *133*, 16754−16757.
(56) Himo, F.; Eriksson, L. A. Theoretical Study of Model Tryptophan Radicals and Radical Cations: Comparison with Experimental Data of DNA Photolyase, Cytochrome *c* Peroxidase, and Ribonucleotide Reductase. *J. Phys. Chem. B* **1997**, *101*, 9811−9819.
(57) Kiryutin, A. S.; Morozova, O. B.; Kuhn, L. T.; Yurkovskaya, A. V.; Hore, P. J. $^{1}$H and $^{13}$C Hyperfine Coupling Constants of the Tryptophanyl Cation Radical in Aqueous Solution from Microsecond Time-Resolved CIDNP. *J. Phys. Chem. B* **2007**, *111*, 11221−11227.


DOI: 10.1021/acs.jpcb.5b06668
*J. Phys. Chem. B* 2015, 119, 13934−13943